3

Power Measurement

Pasquale Arpaia
Università di Napoli Federico II

Francesco Avallone
Università di Napoli Federico II

Aldo Baccigalupi
Università di Napoli Federico II

Claudio de Capua
Università di Napoli Federico II

Carmine Landi
Università de L'Aquila

In this chapter, the concept of electric power is first introduced, and then the most popular power measurement methods and instruments in *dc, ac*, and *pulse* waveform circuits are illustrated.

Power is defined as the *work performed per unit time.* So, dimensionally, it is expressed as joules per second, J s^{-1}. According to this general definition, electric power is the electric work or energy dissipated per unit time and, dimensionally, it yields:

$$\mathrm{J\,s^{-1}} = \mathrm{J\,C^{-1}} \times \mathrm{C\,s^{-1}} = \mathrm{V} \times \mathrm{A} \tag{3.1}$$

where J = Joules
s = Seconds
C = Coulombs
V = Volts
A = Amperes

The product *voltage times current* gives an electrical quantity equivalent to *power.*

3.1 Power Measurements in Dc Circuits

Electric power (P) dissipated by a load (L) fed by a dc power supply (E) is the product of the voltage across the load (V_L) and the current flowing in it (I_L):

$$P = V_L \times I_L \tag{3.2}$$

Therefore, a power measurement in a dc circuit can be generally carried out using a voltmeter (V) and an ammeter (A) according to one of the arrangements shown in Figure 3.1. In the arrangement of Figure 3.1(a), the ammeter measures the current flowing into the voltmeter, as well as that into the load; whereas in the arrangement of Figure 3.1(b), this error is avoided, but the voltmeter measures the voltage drop across the ammeter in addition to that dropping across the load. Thus, both arrangements give a surplus of power measurement absorbed by the instruments. The corresponding measurement errors are generally referred to as insertion errors.

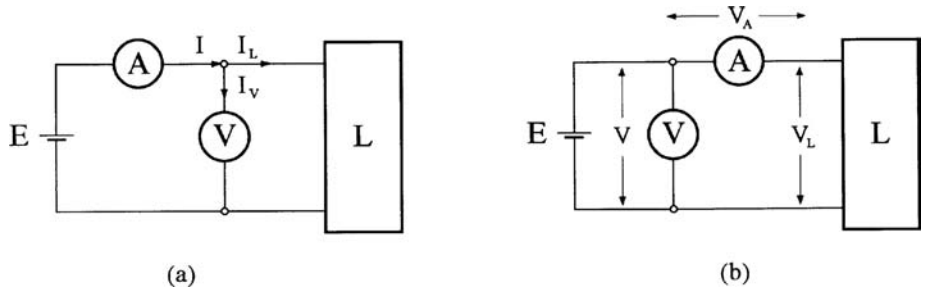

FIGURE 3.1 Two arrangements for dc power measurement circuits.

According to the notation:

- I, Current measured by the ammeter (Figure 3.1(a))
- V, Voltage measured by the voltmeter (Figure 3.1(b))
- R_V, R_A, Internal resistance of the voltmeter and the ammeter, respectively
- R_L, Load resistance
- I_V Current flowing into the voltmeter (Figure 3.1(a))
- V_A, Voltage drop across the ammeter (Figure 3.1(b))

the following expressions between the measurand electric power P and the measured power $V \times I$ are derived by analyzing the circuits of Figures 3.1(a) and 3.1(b), respectively:

$$P = V_L \times I_L = V \times I \times \left(\frac{R_V - R_L}{R_V} \right) \tag{3.3}$$

$$P = V_L \times I_L = V \times I \times \left(\frac{R_L - R_A}{R_L} \right) \tag{3.4}$$

If:

- I_V, compared with I
- V_A, compared with V

are neglected for the arrangements of Figure 3.1(a) and 3.1(b), respectively, it approximately yields:

$$\frac{I_V}{I} = \frac{R_L}{R_V + R_L} \cong \frac{R_L}{R_V} \cong 0; \quad \frac{V_A}{V} \cong \frac{R_A}{R_A + R_L} \cong \frac{R_A}{R_L} \cong 0; \tag{3.5}$$

consequently, measured and measurand power will be coincident.

On this basis, from Equations 3.3, 3.4, and 3.5, analytical corrections of the insertion errors can be easily derived for the arrangement of Figures 3.1(a) and 3.1(b), respectively.

The instrument most commonly used for power measurement is the *dynamometer.* It is built by (1) two fixed coils, connected in series and positioned coaxially with space between them, and (2) a moving coil, placed between the fixed coils and equipped with a pointer (Figure 3.2(a)).

The torque produced in the dynamometer is proportional to the product of the current flowing into the fixed coils times that in the moving coil. The fixed coils, generally referred to as *current coils,* carry the load current while the moving coil, generally referred to as *voltage coil,* carries a current that is proportional, via the multiplier resistor R_V, to the voltage across the load resistor R_L. As a consequence, the deflection of the moving coil is proportional to the power dissipated into the load.

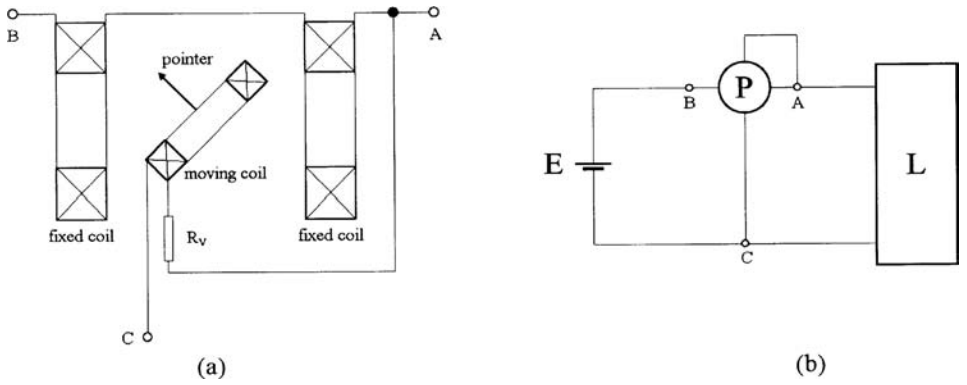

FIGURE 3.2 Power measurement with a dynamometer. (a) Working principle; (b) measurement circuit.

As for the case of Figure 3.1, insertion errors are also present in the dynamometer power measurement. In particular, by connecting the voltage coil between A and C (Figure 3.2(b)), the current coils carry the surplus current flowing into the voltage coil. Consequently, the power P_L dissipated in the load can be obtained by the dynamometer reading P as:

$$P_L = P - \frac{V^2}{R'_v} \tag{3.6}$$

where R'_v is the resistance of the voltage circuit ($R'_v = R_v + R_{vc}$, where R_{vc} is the resistance of the voltage coil). By connecting the moving coil between B and C, this current error can be avoided, but now the voltage coil measures the surplus voltage drop across the current coils. In this case, the corrected value is:

$$P_L = P - I^2 R_C \tag{3.7}$$

where R_C is the resistance of the current coil.

3.2 Power Measurements in Ac Circuits

Definitions

All the above considerations relate to *dc* power supplies. Now look at power dissipation in *ac* fed circuits. In this case, electric power, defined as voltage drop across the load times the current flowing through it, is the function:

$$p(t) = v(t) \times i(t) \tag{3.8}$$

referred to as the *instantaneous power*. In ac circuits, one is mainly interested in the mean value of instantaneous power for a defined time interval. In circuits fed by periodic ac voltages, it is relevant to define the mean power dissipated in one period T (*active power* P):

$$P = \frac{1}{T}\int_0^T p(t)\,dt \tag{3.9}$$

The simplest case is a sinusoidal power supply feeding a purely resistive load. In this case, $v(t)$ and $i(t)$ are in phase and $p(t)$ is given by:

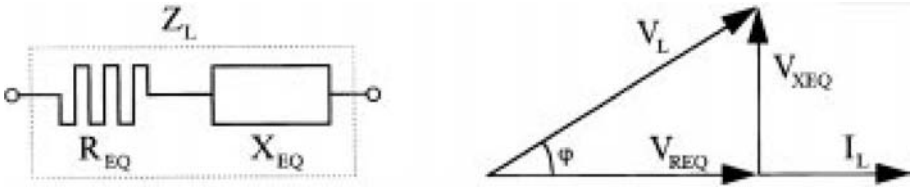

FIGURE 3.3 Voltage drop on the load and on its equivalent components.

$$p(t) = VI\left[1 - \cos(2\omega t)\right] \tag{3.10}$$

where V and I = rms values of $v(t)$ and $i(t)$, respectively
ω = power supply angular frequency

Therefore, the instantaneous power is given by a constant value VI plus the ac quantity oscillating with twice the angular frequency of the power supply; thus, the active power is simply the product VI. In this case, all the above considerations referring to active power for dc circuits are still correct, but voltages and currents must be replaced by the corresponding rms values.

The case of purely reactive loads is the opposite; the voltage drop across the load and current flowing through it are out of phase by 90°. Instantaneous power $p(t)$ is given by:

$$p(t) = VI\cos(2\omega t) \tag{3.11}$$

Thus, the active power dissipated by a reactive load is zero, owing to the phase introduced by the load itself between voltage and current.

The simplest cases of sinusoidal power sources supplying purely resistive and purely reactive loads have been discussed. In these cases, the load is expressed by a real or a pure imaginary number. In general, the load is represented by a complex quantity (the impedance value). In this case, load impedance can be represented by its equivalent circuit (e.g., a pure resistance and a pure reactance in series). With this representation in mind, the electric power dissipated in the load Z_L (Figure 3.3) can be expressed by the sum of power components separately dissipated by resistance R_{EQ} and reactance X_{EQ} of the equivalent circuit Z_L.

Considering that no active power is dissipated in the reactance X_{EQ}, it yields:

$$P = V_{REQ} I_L = V_L I_L \cos\varphi \tag{3.12}$$

The term cosφ appearing in Equation 3.12 is referred to as the *power factor*. It considers that only a fraction of voltage V_L contributes to the power; in fact, its component V_{XEQ} (the drop across the reactance) does not produce any active power, as it is orthogonal to the current I_L flowing into the load.

Figure 3.4 plots the waveforms of instantaneous power $p(t)$, voltage $v(t)$, and current $i(t)$. The effect of the power factor is demonstrated by a dc component of $p(t)$ that varies from a null value (i.e., $v(t)$ and $i(t)$ displaced by 90°) toward the value VI (i.e., $v(t)$ and $i(t)$ in phase).

The term:

$$P_A = V_L I_L \tag{3.13}$$

is called the *apparent power*, while the term:

$$Q = V_{XEQ} I_L = V_L I_L \sin\varphi \tag{3.14}$$

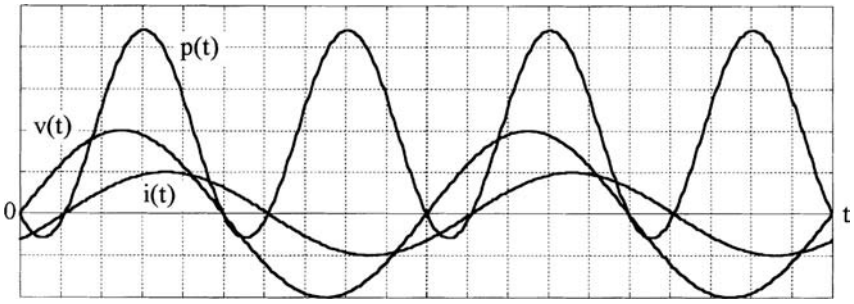

FIGURE 3.4 Waveforms of instantaneous power (p), voltage (v), and current (i).

is called the *reactive power* because it represents a quantity that is dimensionally equivalent to power. This is introduced as a consequence of the voltage drop across a pure reactance and, therefore, does not give any contribution to the active power. From Figure 3.3, the relationship existing between *apparent power*, *active power*, and *reactive power* is given by:

$$P_A = \sqrt{P^2 + Q^2} \tag{3.15}$$

Dynamometers working in ac circuits are designed to integrate instantaneous power according to Equation 3.9. Insertion errors can be derived by simple considerations analogous to the dc case. However, in ac, a phase uncertainty due to the not purely resistive characteristic of voltage circuit arises. In sinusoidal conditions, if ε_w (in radians) is the phase of the real coil impedance, and $\cos\varphi$ is the load power factor, the relative uncertainty in active power measurements can be shown to be equal to $-\varepsilon_w T_g \varphi$. The phase uncertainty depends on the frequency. By using more complex circuits, the frequency range of the dynamometer can be extended to a few tens of kilohertz.

The above has presented the power definitions applied to ac circuits with the restrictions of sinusoidal quantities. In the most general case of distorted quantities, obviously symbolic representation can no longer be applied. In any case, active power is always defined as the mean power dissipated in one period.

As far as methods and instruments for ac power measurements are concerned, some circuit classification is required. In fact, the problems are different, arising in circuits as the frequency of power supply increases. Therefore, in the following, ac circuits will be classified into (1) line-frequency circuits, (2) low- and medium-frequency circuits (up to a few megahertz), and (3) high-frequency circuits (up to a few gigahertz). Line-frequency circuits will be discussed separately from low-frequency circuits, principally because of the existence of problems related specifically to the three-phase power supply of the main.

Low- and Medium-Frequency Power Measurements

In the following, the main methods and instruments for power measurements at low and medium frequencies are considered.

Three-Voltmeter Method

The power dissipation in the load L can be measured using a noninductive resistor R and measuring the three voltages shown in Figure 3.5 [1]. Although one of the voltages might appear redundant on a first analysis of the circuit, in actual fact, three independent data are needed in order to derive power from Equation 3.12. In particular, from voltage drops v_{AB} and v_{BC}, the load current and load voltage can be directly derived; instead, v_{AC} is used to retrieve information about their relative phase.

If currents derived by voltmeters are neglected and the current i_L flowing into the load L is assumed to be equal to that flowing into the resistor R, the statement can be demonstrated as follows:

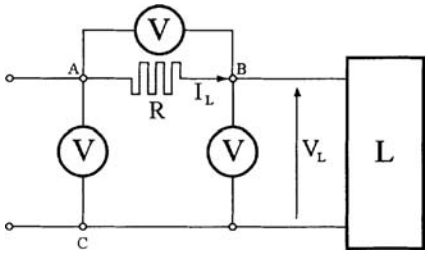

FIGURE 3.5 Three-voltmeter method.

$$v_{AC} = v_L + Ri_L$$
$$v_{AC}^2 = R^2 i_L^2 + v_L^2 + 2Rv_L i_L \tag{3.16}$$

where the small characters indicate instantaneous values. By computing rms values (indicated as capital characters), one obtains the power P_L:

$$\frac{1}{T}\int_0^T v_{AC}^2 dt = \frac{1}{T}\int_0^T R^2 i_L^2 dt = \frac{1}{T}\int_0^T v_L^2 dt + \frac{1}{T}\int_0^T 2Rv_L i_L dt$$
$$V_{AC}^2 = RI_L^2 + V_L^2 + 2RP_L \tag{3.17}$$
$$P_L = \frac{V_{AC}^2 - R^2 I_L^2 - V_L^2}{2R} = \frac{V_{AC}^2 - V_{AB}^2 - V_{BC}^2}{2R}$$

Equation 3.17 is also the same in dc by replacing rms values with dc values. Since the result is obtained as a difference, problems arise from relative uncertainty when the three terms have about sum equal to zero.

Such a method is still used for high-accuracy applications.

Thermal Wattmeters

The working principle of thermal wattmeters is based on a couple of twin thermocouples whose output voltage is proportional to the square of the rms value of the currents flowing into the thermocouple heaters [2].

The principle circuit of a thermal wattmeter is shown in Figure 3.6(a). Without the load, with the hypothesis $S \ll r_1$ and $S \ll r_2$, the two heaters are connected in parallel and, if they have equal resistance r ($r_1 = r_2 = r$), they are polarized by the same current i_p

$$i_1 = i_2 = \frac{i_p}{2} = \frac{v}{2R + r} \tag{3.18}$$

In this case, the output voltages of the two thermocouples turn out to be equal ($e_1 = e_2$); thus, the voltage Δe measured by the voltmeter is null. In Figure 3.6(b), this situation is highlighted by the working point T equal for both thermocouples. By applying a load L with a corresponding current i_L, a voltage drop across S arises, causing an imbalance between currents i_1 and i_2. With the hypothesis that $r \ll R$, the two heaters are in series; thus, the current imbalance through them is:

$$i_1 - i_2 = \frac{Si_L}{2R} \tag{3.19}$$

This imbalance increases the current i_1 and decreases i_2. Therefore, the working points of the two thermocouples change: the thermocouple polarized by the current i_1 operates at A, and the other thermocouple

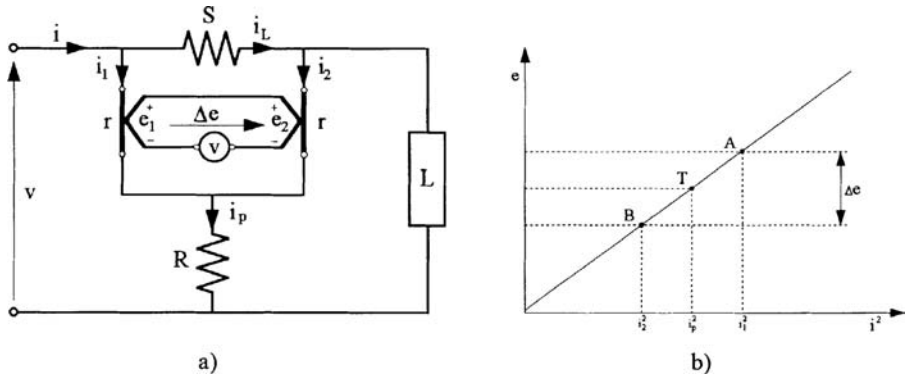

FIGURE 3.6 Thermal wattmeter based on twin thermocouples (*a*); working characteristic in ideal conditions (*b*).

operates at B (Figure 3.6(b)). In this situation, with the above hypotheses, the voltmeter measures the voltage imbalance Δe proportional to the active power absorbed by the load (except for the surplus given by the powers dissipated in R, S, r_1, and r_2):

$$\begin{aligned}\Delta e &= k\left(\left\langle i_1^2\right\rangle - \left\langle i_2^2\right\rangle\right) = k\left(\left\langle\left(i_p + i_L\right)^2\right\rangle - \left\langle\left(i_p - i_L\right)^2\right\rangle\right) \\ &= k\left\langle 4 i_p i_L\right\rangle = k_1\left\langle v(t) i(t)\right\rangle = k_1 P\end{aligned} \tag{3.20}$$

where the notation $\langle i \rangle$ indicates the time average of the quantity i.

If the two thermocouples cannot be considered as twins and linear, the power measurement accuracy will be obviously compromised. This situation is shown in Figure 3.7 where the two thermocouples are supposed to have two quite different nonlinear characteristics. In this case, the voltage measured by voltmeter will be Δe_n instead of Δe.

Wattmeters based on thermal principle allow high accuracy to be achieved in critical cases of highly distorted wide-band spectrum signals.

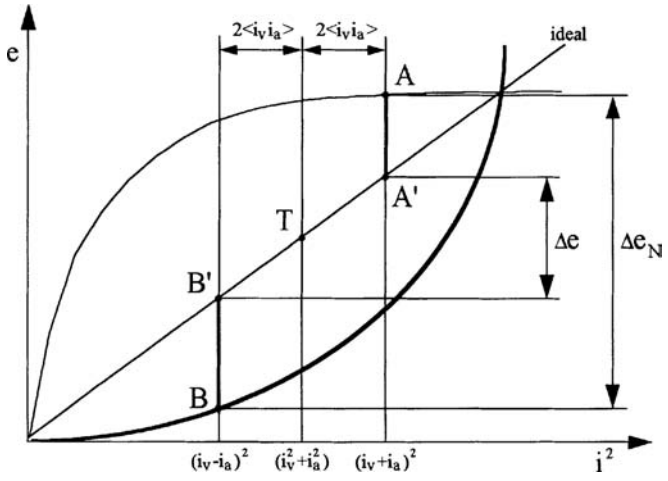

FIGURE 3.7 Ideal and actual characteristics of thermal wattmeter thermocouples.

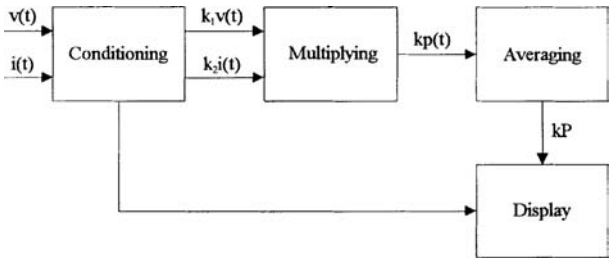

FIGURE 3.8 Block diagram of a multiplier-based wattmeter.

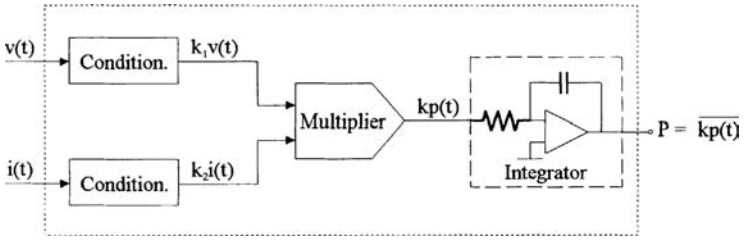

FIGURE 3.9 Block diagram of a four-quadrant, multiplier-based wattmeter.

Wattmeters Based on Multipliers

The multiplication and averaging processes (Figure 3.8) involved in power measurements can be undertaken by electronic means.

Electronic wattmeters fall into two categories, depending on whether multiplication and averaging operations are performed in a continuous or discrete way. In continuous methods, multiplications are mainly carried out by means of analog electronic multipliers. In discrete methods, sampling wattmeters take simultaneous samples of voltage and current waveforms, digitize these values, and provide multiplication and averaging using digital techniques.

Analogous to the case of dynamometers, the resistances of the voltage and current circuits have to be taken into account (see Equations 3.6 and 3.7). Also, phase errors of both current ε_{wc} and voltage ε_{wv} circuits increase the relative uncertainty of power measurement, e.g., in case of sinusoidal conditions increased at $(\varepsilon_{wc}-\varepsilon_{wv})T_g\varphi$.

Wattmeters Based on Analog Multipliers

The main analog multipliers are based on a transistor-based popular circuit such as a four-quadrant multiplier [3], which processes voltage and current to give the instantaneous power, and an integrator to provide the mean power (Figure 3.9). More effective solutions are based on (1) Time Division Multipliers (TDMs), and (2) Hall effect-based multipliers.

TDM-Based Wattmeters.

The block diagram of a wattmeter based on a TDM is shown in Figure 3.10 [4]. A square wave v_m (Figure 3.11(a)) with constant period T_g, and duty cycle and amplitude determined by $i(t)$ and $v(t)$, respectively, is generated. If T_g is much smaller than the period of measurands $v_x(t)$ and $v_y(t)$, these voltages can be considered as constant during this time interval.

The duty cycle of v_m is set by an impulse duration modulator circuit (Figure 3.10). The ramp voltage $v_g(t)$ (Figure 3.11(b)) is compared to the voltage $v_y(t)$ proportional to $i(t)$, and a time interval t_2, whose duration is proportional to $v_y(t)$, is determined. If

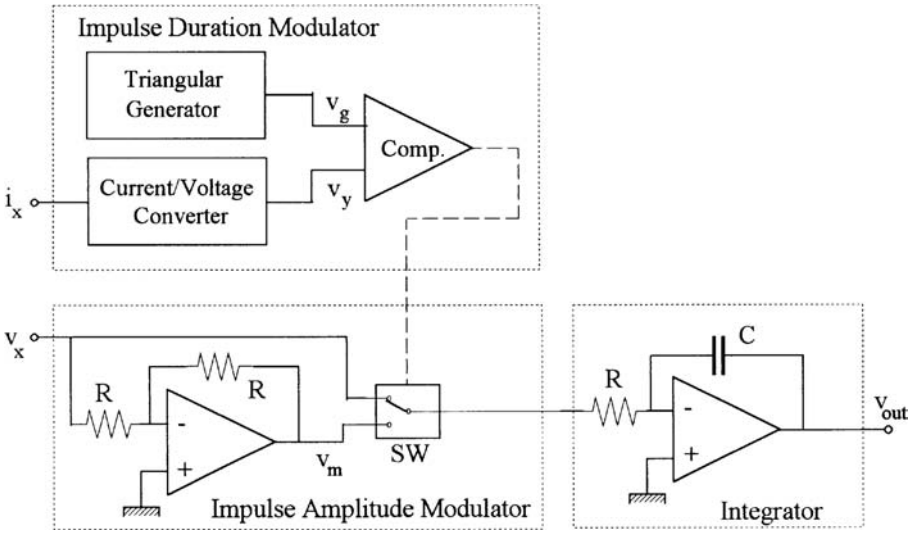

FIGURE 3.10 Block diagram of a TDM-based wattmeter.

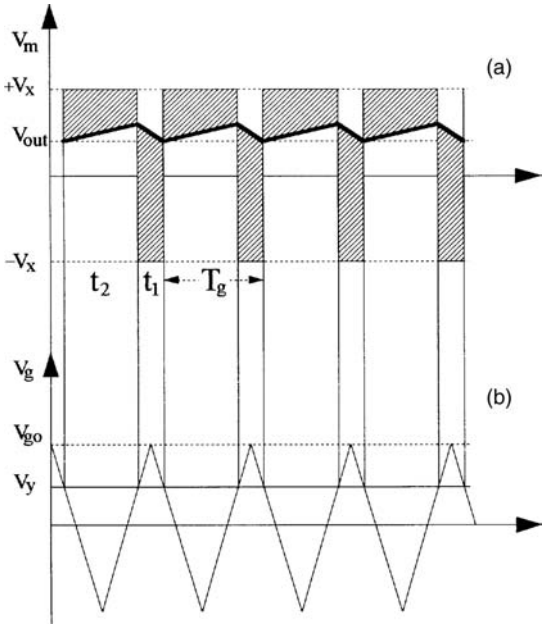

FIGURE 3.11 Waveform of the TDM-based power measurement: (*a*) impulse amplitude modulator output, (*b*) ramp generator output.

$$v_g(t) = \frac{4V_{g0}}{T_g}t \quad \text{when} \quad 0 \le t \le \frac{T_g}{4} \tag{3.21}$$

then from simple geometrical considerations, one obtains:

$$t_2 = 2\left(\frac{T_g}{4} - \frac{v_y T_g}{4V_{g0}}\right) \tag{3.22}$$

and

$$t_1 - t_2 = \frac{T_g}{V_{g0}} v_y \tag{3.23}$$

The amplitude of $v_m(t)$ is set by an impulse amplitude modulator circuit. The output square wave of the impulse duration modulator drives the output $v_m(t)$ of the switch SW to be equal to $+v_x$ during the time interval t_1, and to $-v_x$ during the time interval t_2 (Figure 3.11(a)).

Then, after an initial transient, the output voltage $v_{out}(t)$ of the low-pass filter (integrator) is the mean value of $v_m(t)$:

$$V_{out} = \frac{1}{RC}\int_0^t v_m(t)dt = K'\left(\int_0^{t1} v_x(t)dt - \int_{t1}^{t1+t2} v_x(t)dt\right) = K'v_x(t_1 - t_2) = Kv_x v_y \tag{3.24}$$

The high-frequency limit of this wattmeter is determined by the low-pass filter and it must be smaller than half of the frequency of the signal $v_g(t)$. The frequency limit is generally between 200 Hz and 20 kHz, and can reach 100 kHz. Uncertainties are typically 0.01 to 0.02% [5].

Hall Effect-Based Wattmeters.

As is well known, in a Hall-effect transducer, the voltage $v_H(t)$ is proportional to the product of two time-dependent quantities [6]:

$$v_H(t) = R_H i(t) B_t \tag{3.25}$$

where R_H = Hall constant
$i(t)$ = Current through the transducer
$B(t)$ = Magnetic induction

In the circuit of Figure 3.12(a), the power P is determined by measuring $v_H(t)$ through a high-input impedance averaging voltmeter, and by considering that $v_x(t) = ai(t)$ and $i_x(t) = bB(t)$, where a and b are proportionality factors:

$$P = \frac{1}{T}\int_0^T v_x(t)\cdot i_x(t)\mathrm{d}t = ab\frac{1}{T}\int_0^T i(t)\cdot B(t)\mathrm{d}t = abR_H V_H \tag{3.26}$$

where T is the measurand period, and V_H the mean value of $v_H(t)$.

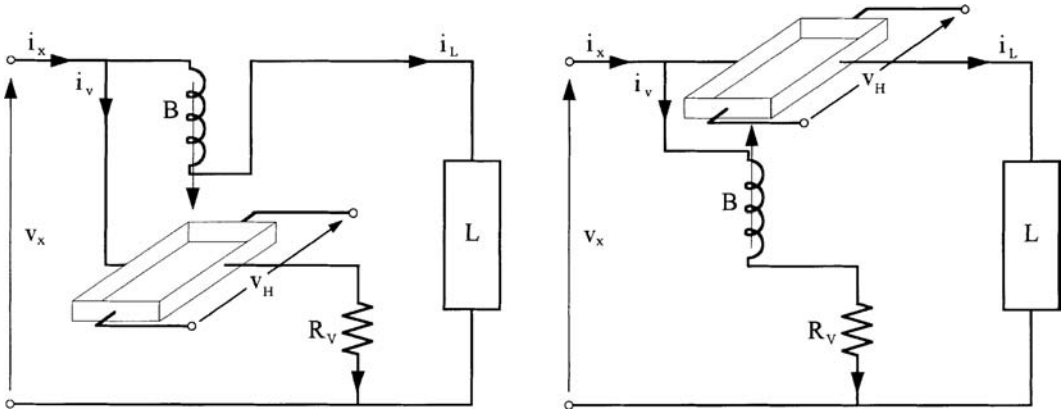

FIGURE 3.12 Configurations of the Hall effect-based wattmeter.

In the usual realization of the Hall multiplier (0.1% up to a few megahertz), shown in Figure 3.12(a), the magnetic induction is proportional to the load current and the optimal polarizing current i_v is set by the resistor R_v.

For the frequency range up to megahertz, an alternative arrangement is shown in Figure 3.12(b), in which the load current I_L flows directly into the Hall device, acting as a polarizing current, and the magnetic field is generated by the voltage *v*. In this same way, the temperature influence is reduced for line-frequency applications with constant-amplitude voltages and variable load currents.

In the megahertz to gigahertz range, standard wattmeters use probes in waveguides with rectifiers.

Wattmeters Based on Digital Multipliers

Sampling Wattmeters.

The most important wattmeter operating on discrete samples is the sampling wattmeter (Figure 3.13). It is essentially composed of two analog-to-digital input channels, each constituted by (1) a conditioner (C), (2) a sample/hold (S/H), (3) an analog-to-digital converter (ADC), (4) a digital multiplier (MUL), and (5) summing (SUM), dividing (DIV), and displaying units (DISP). The architecture is handled by a processing unit not shown in Figure 3.13.

If samples are equally spaced, the active power is evaluated as the mean of the sequence of instantaneous power samples $p(k)$:

$$\bar{p} = \frac{1}{N}\sum_{k=0}^{N-1} p(k) = \frac{1}{N}\sum_{k=0}^{N-1} v(k)i(k) \tag{3.27}$$

where N^* represents the number of samples in one period of the input signal, and $v(k)$ and $i(k)$ are the kth samples of voltage and current, respectively. A previous estimation of the measurand fundamental period is made to adjust the summation interval of Equation 3.27 and/or the sampling period in order to carry out a synchronous sampling [7]. The sampling period can be adjusted by using a frequency multiplier with PLL circuit driven by the input signal [8]. Alternatively, the contribution of the sampling error is reduced by carrying out the mean on a high number of periods of the input signal.

In the time domain, the period estimation of highly distorted signals, such as Pulse Width Modulation (PWM), is made difficult by the numerous zero crossings present in the waveform. Some types of digital filters can be used for this purpose. An efficient digital way to estimate the period is the discrete integration of the PWM signal. In this way, the period of the fundamental harmonic is estimated by detecting the sign changes of the cumulative sum function [9]:

$$S(k) = \sum_{i=1}^{k} p_i \qquad k = 1, 2, \ldots, N \tag{3.28}$$

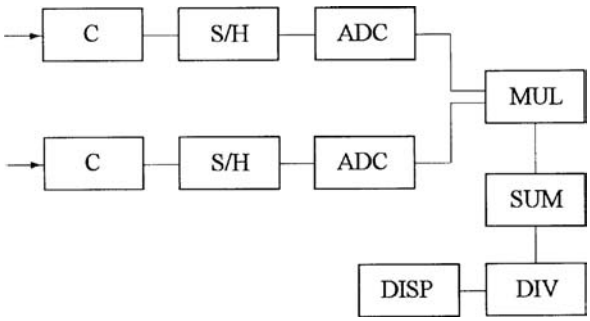

FIGURE 3.13 Block diagram of the sampling wattmeter.

If the summation interval is extended to an integer number of periods of the $S(k)$ function, a "quasisynchronous" sampling [10] is achieved through a few simple operations (cumulative summation and sign detection) and the maximum synchronization error is limited to a sampling period. Through relatively small increases in computational complexity and memory size, the residual error can be further reduced through a suitable data processing algorithm; that is, the multiple convolution in the time domain of triangular windows [9]. Hence, the power measurement can be obtained as:

$$P_{(B)} = \frac{1}{\sum_{k=0}^{2B(N^*-1)} w(k)} \sum_{k=0}^{2B(N^*-1)} w(k)\,p(k) \tag{3.29}$$

where $p(k)$ is the k^{th} sample of the instantaneous power and $w(k)$ the k^{th} weight corresponding to the window obtained as the convolution of B triangular windows [10].

Another way to obtain the mean power is through the consideration of the harmonic components of voltages and currents in the frequency domain using the Discrete Fourier Transform [11]. In particular, a Fast Fourier Transform algorithm is used in order to improve efficiency. Successively, a two-step research of the harmonic peaks is carried out: (1) the indexes of the frequency samples corresponding to the greatest spectral peaks provide a rough estimate of the unknown frequencies when the wide-band noise superimposed onto the signal is below threshold; (2) a more accurate estimate of harmonic frequencies is carried out to determine the fractional bin frequency (i.e., the harmonic determination under the frequency resolution); to this aim, several approaches such as zero padding, interpolation techniques, and flat-top window-based technique can be applied [12].

Line-Frequency Power Measurements

For line applications where the power is directly derived by the source network, the assumption of infinite power source can be reliably made, and at least one of the two quantities voltage or current can be considered as sinusoidal. In this case, the definition of the power as the product of voltage and current means that only the power at the fundamental frequency can be examined [13].

Single-Phase Measurements

Single-phase power measurements at line frequency are carried out by following the criteria previously mentioned. In practical applications, the case of a voltage greater than 1000 V is relevant; measurements must be carried out using voltage and current transformers inserted as in the example of Figure 3.14. The relative uncertainty is equal to:

$$\frac{\Delta P}{P} = \left(\eta_w + \eta_a + \eta_v\right) + \left(\varepsilon_w + \varepsilon_a + \varepsilon_v\right) T_g \varphi_c \tag{3.30}$$

where η_w and ε_w are the instrumental and phase uncertainty of the wattmeter, η_a and η_v are the ratio uncertainties of current (CT) and voltage (VT) transformers, and ε_a and ε_v their phase uncertainties, respectively.

If the load current exceeds the current range of the wattmeter, a current transformer must be used, even in the case of low voltages.

Polyphase Power Measurements

Three-phase systems are the polyphase systems most commonly used in practical industrial applications. In the following, power measurements on three-phase systems will be derived as a particular case of polyphase systems (systems with several wires) and analyzed for increasing costs: (1) balanced and symmetrical systems, (2) three-wire systems, (3) two wattmeter-based measurements, (4) unbalanced systems, (5) three wattmeter-based measurements, and (6) medium-voltage systems.

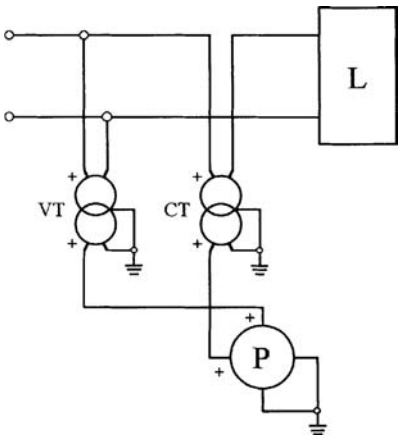

FIGURE 3.14 Single-phase power measurement with voltage (VT) and current (CT) transformers.

Measurements on Systems with Several Wires

Consider a network with sinusoidal voltages and currents composed by n wires. For the currents flowing in such wires, the following relation is established:

$$\sum_{1}^{n} \dot{I}_{\mathrm{i}} = 0 \tag{3.31}$$

The network can be thought as composed of $n-1$ single-phase independent systems, with the common return on any one of the wires (e.g., the s^{th} wire). Then, the absorbed power can be measured as the sum of the readings of $n-1$ wattmeters, each one inserted with the current circuit on a different wire and the voltmeter circuit between such a wire and the s^{th} one (Figure 3.15):

$$P = \sum_{1}^{n-1} \left(\dot{V}_{\mathrm{is}} \times \dot{I}_{\mathrm{i}} \right) \tag{3.32}$$

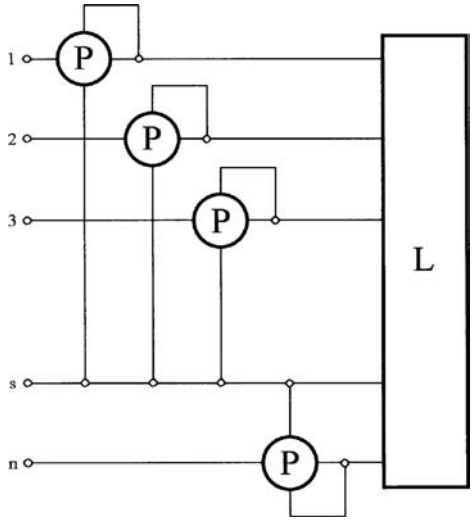

FIGURE 3.15 Power measurement on systems with several wires.

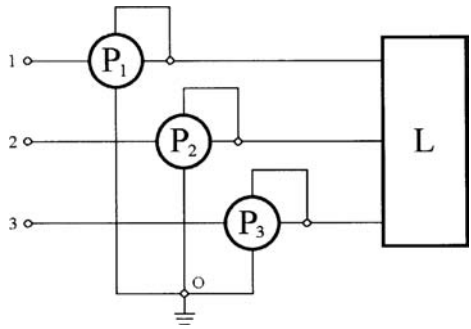

FIGURE 3.16 Power measurement on three-wire systems.

The absorbed power can be also measured by referring to a generic point O external to the network. In this case, the absorbed power will be the sum of the readings of n wattmeters, each inserted with the ammeter circuit on a different wire and the voltmeter circuit connected between such a wire and the point O:

$$P = \sum_{1}^{n} \left(\dot{V}_{io} \times \dot{I}_{i} \right) \tag{3.33}$$

Power Measurements on Three-Wire Systems

Active power in a three-phase power system can generally be evaluated by three wattmeters connected as shown in Figure 3.16.

For each power meter, the current lead is connected on a phase wire and the voltmeter lead is connected between the same wire and an artificial neutral point O, whose position is fixed by the voltmeter impedance of power meters or by suitable external impedances.

Under these conditions, absorbed power will be the sum of the three wattmeter indications:

$$P = \sum_{1}^{3} \left(\dot{V}_{io} \times \dot{I}_{i} \right) \tag{3.34}$$

If the three-phase system is provided by four wires (three phases with a neutral wire), the neutral wire is utilized as a common wire.

Symmetrical and Balanced Systems

The supply system is symmetrical and the three-phase load is balanced; that is:

$$\begin{cases} V_1 = V_2 = V_3 \\ I_1 = I_2 = I_3 \end{cases} \tag{3.35}$$

In Figure 3.17, the three possible kinds of insertion of an instrument S (an active power or a reactive power meter) are illustrated. The first (a in Figure 3.17) was described in the last subsection; if S is a wattmeter; the overall active power is given by three times its indication, and similarly for the reactive power if S is a reactive power meter. Notice that a couple of twin resistors with the same resistance R of the voltage circuit of S are placed on the other phases to balance the load.

The other two insertions are indicated by the following convention: S_{ijk} indicates a reading performed with the current leads connected to the line "i" and the voltmeter leads connected between the phases "j" and "k." If "i" is equal to "j", one is omitted (e.g., the notation P_{12} (b in Figure 3.17)). The active power absorbed by a single phase is usually referred to as P_1.

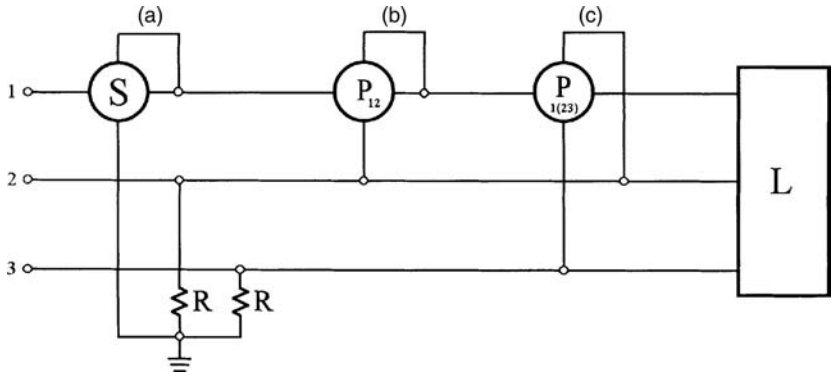

FIGURE 3.17 The three kinds of insertion of a power meter.

The wattmeter reading corresponding to the (c) case in Figure 3.17 is equal to the reactive power Q_1 involved in phase 1, save for the factor $\sqrt{3}$. Hence, in the case of symmetrical and balanced systems, the overall reactive power is given by:

$$Q = 3Q_1 = 3P_{1(23)} \Big/ \sqrt{3} = \sqrt{3}\, P_{1(23)} \tag{3.36}$$

In fact, one has:

$$P_{1(23)} = \dot{I}_1 \times \dot{V}_{23} \tag{3.37}$$

but:

$$\dot{V}_{12} + \dot{V}_{23} + \dot{V}_{31} = 0 \;\Rightarrow\; P_{1(23)} = \dot{I}_1 \times \left(-\dot{V}_{12} - \dot{V}_{31}\right)$$

$$\dot{V}_{13} = -\dot{V}_{31} \;\Rightarrow\; P_{1(23)} = -\dot{I}_1 \times \dot{V}_{12} + \dot{I}_1 \times \dot{V}_3$$

$$\begin{cases} \dot{I}_1 \times \dot{V}_{12} = P_{12} \\ \dot{I}_1 \times \dot{V}_{13} = P_{13} \end{cases} \Rightarrow\; P_{1(23)} = P_{13} - P_{12}$$

In the same manner, the following relationships, which are valid for any kind of supply and load, can be all proved:

$$\begin{aligned} P_{1(23)} &= P_{13} - P_{12} \\ P_{2(31)} &= P_{21} - P_{23} \\ P_{3(12)} &= P_{32} - P_{31} \end{aligned} \tag{3.38}$$

If the supply system is symmetrical, $P_{1(23)} = \sqrt{3}Q_1$.
In fact, moving from the relationship (Figure 3.18):

$$P_{1(23)} = \dot{I}_1 \times \dot{V}_{23} = I_1 V_{23} \cos\beta \tag{3.39}$$

where $\beta = 90° - \varphi_1$, one obtains $P_{1(23)} = \sqrt{3}E_1 I_1 \sin\varphi_1 = \sqrt{3}Q_1$.

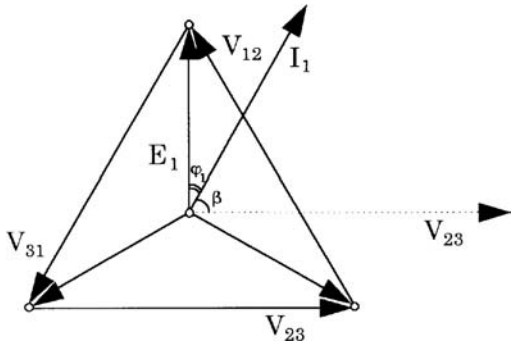

FIGURE 3.18 Phasor diagram for a three-phase symmetrical and balanced system.

In the same manner, the other two corresponding relationships for $P_{2(31)}$ and $P_{3(12)}$ are derived. Hence:

$$\begin{aligned} P_{1(23)} &= \sqrt{3}Q_1 = P_{13} - P_{12} \\ P_{2(31)} &= \sqrt{3}Q_2 = P_{21} - P_{23} \\ P_{3(12)} &= \sqrt{3}Q_3 = P_{32} - P_{31} \end{aligned} \tag{3.40}$$

Power Measurements Using Two Wattmeters

The overall active power absorbed by a three-wire system can be measured using only two wattmeters. In fact, Aron's theorem states the following relationships:

$$\begin{aligned} P &= P_{12} + P_{32} \\ P &= P_{23} + P_{13} \\ P &= P_{31} + P_{21} \end{aligned} \tag{3.41}$$

Analogously, the overall reactive power can be measured by using only two reactive power meters:

$$\begin{aligned} Q &= Q_{12} + Q_{32} \\ Q &= Q_{23} + Q_{13} \\ Q &= Q_{31} + Q_{21} \end{aligned} \tag{3.42}$$

Here one of the previous statements, that is:

$$P = P_{12} + P_{32}$$

is proved. The two wattmeters connected as shown in Figure 3.19 furnish P_{12}, P_{32}:

Hence, the sum of the two readings gives:

$$\begin{aligned} P_{12} + P_{32} &= \dot{I}_1 \times \dot{V}_{12} + \dot{I}_3 \times \dot{V}_{32} = \dot{I}_1 \times \left(\dot{E}_1 - \dot{E}_2\right) + \dot{I}_3 \times \left(\dot{E}_3 - \dot{E}_2\right) \\ &= \dot{I}_1 \times \dot{E}_1 - \dot{I}_1 \times \dot{E}_2 + \dot{I}_3 \times \dot{E}_3 - \dot{I}_3 \times \dot{E}_2 = \dot{I}_1 \times \dot{E}_1 + \dot{I}_3 \times \dot{E}_3 - \left(\dot{I}_1 + \dot{I}_3\right) \times \dot{E}_2 \\ &= \dot{I}_1 \times \dot{E}_1 + \dot{I}_3 \times \dot{E}_3 + \dot{I}_2 \times \dot{E}_2 = P_1 + P_2 + P_3 = P \end{aligned} \tag{3.43}$$

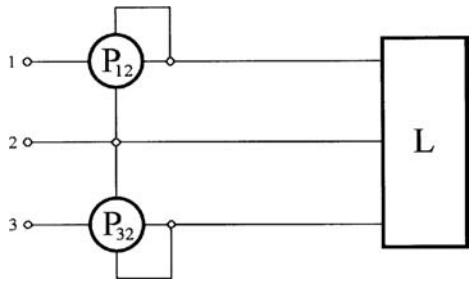

FIGURE 3.19 Power measurements using two wattmeters.

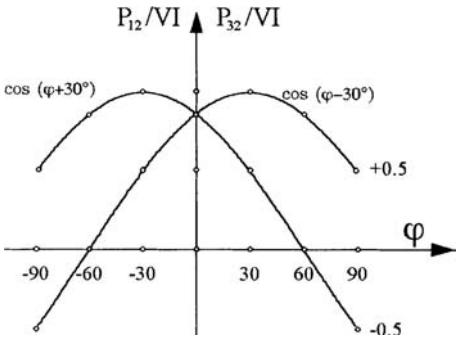

FIGURE 3.20 Sign of powers in Aron insertion.

Provided that the system has only three wires, Aron's theorem applies to any kind of supply and load. In the case of symmetrical and balanced systems, it also allows the reactive power to be evaluated:

$$Q = \sqrt{3} \cdot \left(P_{32} - P_{12}\right) \tag{3.44}$$

Using Equations 3.41 and 3.44, the power factor is:

$$\cos\varphi = \frac{P_{12} + P_{32}}{\sqrt{\left(P_{12} + P_{32}\right)^2 + 3\left(P_{32} - P_{12}\right)^2}} = \frac{P_{12} + P_{32}}{\sqrt{4P_{12}^2 + 4P_{32}^2 - 4P_{12}P_{32}}} = \frac{1 + \dfrac{P_{12}}{P_{32}}}{2\sqrt{\left(\dfrac{P_{12}}{P_{32}}\right)^2 - \left(\dfrac{P_{12}}{P_{32}}\right) + 1}} \tag{3.45}$$

Aron's insertion cannot be utilized when the power factor is low. In fact, if the functions:

$$\begin{aligned} \cos\left(\varphi + 30\right) &= \frac{P_{12}}{VI} \\ \cos\left(\varphi - 30\right) &= \frac{P_{32}}{VI} \end{aligned} \tag{3.46}$$

are considered (Figure 3.20), it can be argued that: (1) for $\varphi \le 60°$, P_{12} and P_{32} are both greater than zero; (2) for $\varphi > 60°$, $\cos(\varphi - 30)$ is still greater than zero, and $\cos(\varphi + 30)$ is lower than zero.

The absolute error in the active power is:

$$\Delta P = \frac{\partial\left(P_{12} + P_{32}\right)}{\partial P_{12}}\Delta P_{12} + \frac{\partial\left(P_{12} + P_{32}\right)}{\partial P_{32}}\Delta P_{32} = \Delta P_{12} + \Delta P_{32} \tag{3.47}$$

This corresponding relative error is greater as P_{12} and P_{32} have values closer to each other and are opposite in polarity; in particular, for $\cos\varphi = 0$ ($\varphi = 90°$), the error is infinite.

If η_w and ε_w are the wattmeter amplitude and phase errors, respectively, then the error in the active power is:

$$\frac{\Delta P}{P} = \frac{\left(\eta_w + \varepsilon_w T_g \varphi_{12}\right) P_{12} + \left(\eta_w + \varepsilon_w T_g \varphi_{32}\right) P_{32}}{P_{12} + P_{32}} = \eta_w + \varepsilon_w \frac{Q}{P} \tag{3.48}$$

Let two wattmeters with nominal values V_0, I_0, $\cos\varphi_0$, and class c be considered; the maximum absolute error in each reading is:

$$\Delta P = \frac{cV_0 I_0 \cos\varphi_0}{100} \tag{3.49}$$

Therefore, the percentage error related to the sum of the two indications is:

$$\frac{\Delta P}{P} = \frac{cV_0 I_0 \cos\varphi_0}{\sqrt{3} VI \cos\varphi} = 1.11 \frac{cV_0 I_0 \cos\varphi_0}{VI \cos\varphi} \tag{3.50}$$

equal to approximately the error of only one wattmeter inserted in a single-phase circuit with the same values of I, V, and $\cos\varphi$. Consequently, under the same conditions, the use of two wattmeters involves a measurement uncertainty much lower than that using three wattmeters.

If the Aron insertion is performed via current and voltage transformers, characterized by ratio errors η_a and η_v, and phase errors ε_a and ε_v, respectively, the active power error is:

$$\frac{\Delta P}{P} = \frac{\left(\eta_{TOT} + \varepsilon_{TOT} T_g \varphi_{12}\right) P_{12} + \left(\eta_{TOT} + \varepsilon_{TOT} T_g \varphi_{32}\right) P_{32}}{P_{12} + P_{32}} = \eta_{TOT} + \varepsilon_{TOT} \frac{Q}{P} = \eta_{TOT} + \varepsilon_{TOT} T_g \Phi_c \tag{3.51}$$

where $\cos\Phi_c = $ conventional power factor

$$\left.\begin{aligned} \eta_{TOT} &= \eta_w + \eta_a + \eta_v \\ \varepsilon_{TOT} &= \varepsilon_w + \varepsilon_a + \varepsilon_v \end{aligned}\right\} \text{ the error sums with } \eta_w \text{ and } \varepsilon_w \text{ being the wattmeter errors.}$$

Symmetrical Power Systems Supplying Unbalanced Loads

If the load is unbalanced, the current amplitudes are different from each other and their relative phase is not equal to 120°. Two wattmeters and one voltmeter have to be connected as proposed by Barbagelata [13] (Figure 3.21). The first wattmeter can provide P_{12} and P_{13}, and the second one gives P_{31} and P_{32}.

From the Aron theorem, the active power is:

$$P = P_{12} + P_{32} \tag{3.52}$$

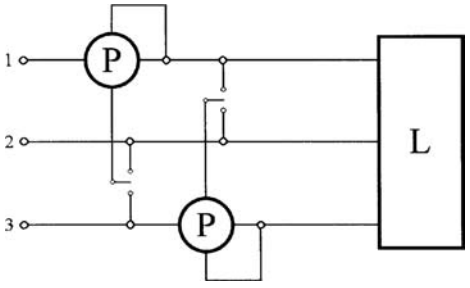

FIGURE 3.21 Barbagelata insertion for symmetrical and unbalanced systems.

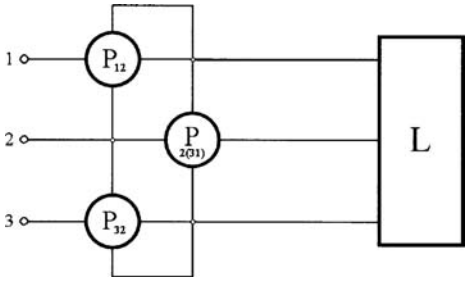

FIGURE 3.22 Righi insertion for symmetrical and unbalanced systems.

and then the reactive power Q is:

$$Q = Q_1 + Q_2 + Q_3 = \frac{1}{\sqrt{3}}\left[P_{13} - P_{12} + \underline{P_{21}} - \underline{P_{23}} + P_{32} - P_{31}\right] \tag{3.53}$$

For the underlined terms, from Aron's theorem it follows that:

$$P = P_{13} + P_{23} = P_{12} + P_{32} = P_{21} + P_{31} \tag{3.54}$$

then:

$$P_{13} + P_{23} = P_{21} + P_{31} \;\Rightarrow\; P_{21} - P_{23} = P_{13} - P_{31}$$

Thus, one obtains:

$$Q = \frac{1}{\sqrt{3}}\left[2\left(P_{13} - P_{31}\right) + P_{32} - P_{12}\right] \tag{3.55}$$

Therefore, using only four power measurements, the overall active and reactive powers can be obtained.

The main disadvantage of this method is that the four measurements are not simultaneous; therefore, any load variations during the measurement would cause a loss in accuracy. In this case, a variation proposed by Righi [13] can be used. In this variation, three wattmeters are connected as shown in Figure 3.22 and give simultaneously P_{12}, P_{32}, and $P_{2(31)}$. Reactive power is:

$$Q = \frac{1}{\sqrt{3}}\left[\underline{P_{13}} - P_{12} + P_{21} - P_{23} + P_{32} - \underline{P_{31}}\right]. \tag{3.56}$$

Analogously as above, from the Aron theorem it follows that:

$$P_{21} - P_{23} = P_{13} - P_{31} \;\Rightarrow\; P_{2(31)} = P_{21} - P_{23} = P_{13} - P_{31} \tag{3.57}$$

then:

$$Q = \frac{1}{\sqrt{3}}\left[P_{32} - P_{12} + 2P_{2(31)}\right] \tag{3.58}$$

For symmetrical and unbalanced systems, another two-wattmeter insertion can be carried out (Figure 3.23). The wattmeters give:

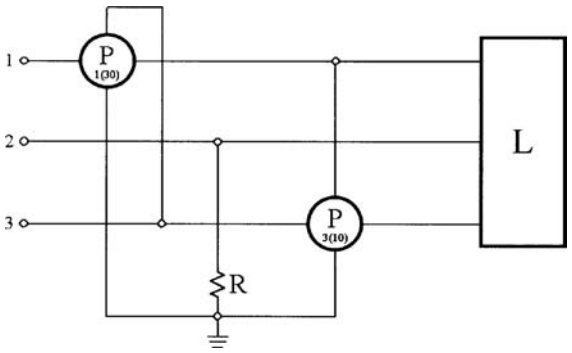

FIGURE 3.23 Two wattmeters-based insertion for symmetrical and unbalanced systems.

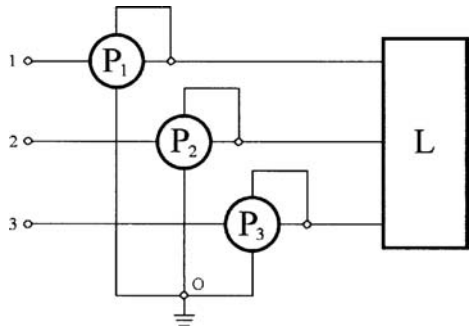

FIGURE 3.24 Three wattmeters-based insertion for three-wire, three-phase systems.

$$P_{1(30)} = \dot{E}_3 \times \dot{I}_1 = j\frac{\dot{V}_{12}}{\sqrt{3}} \times \dot{I}_1 = \frac{Q_{12}}{\sqrt{3}}$$
$$P_{3(10)} = \dot{E}_1 \times \dot{I}_3 = j\frac{\dot{V}_{23}}{\sqrt{3}} \times \dot{I}_3 = \frac{Q_{32}}{\sqrt{3}} \tag{3.59}$$

Hence, the overall reactive power is:

$$Q = Q_{12} + Q_{32} = \sqrt{3}\left[-P_{1(30)} + P_{3(10)}\right] \tag{3.60}$$

Three-Wattmeter Insertion

A three-wire, three-phase system can be measured by three wattmeters connected as in Figure 3.24. The artificial neutral point position does not affect the measurement; it is usually imposed by the impedance of the voltmeter leads of the wattmeters.

Medium-Voltage, Three-Wattmeter Insertion

Analogously to the single-phase case, for medium-voltage circuits, the three-wattmeter insertion is modified as in Figure 3.25.

Method Selection Guide

For three-wire systems, the flow chart of Figure 3.26 leads to selecting the most suitable method according to system characteristics.

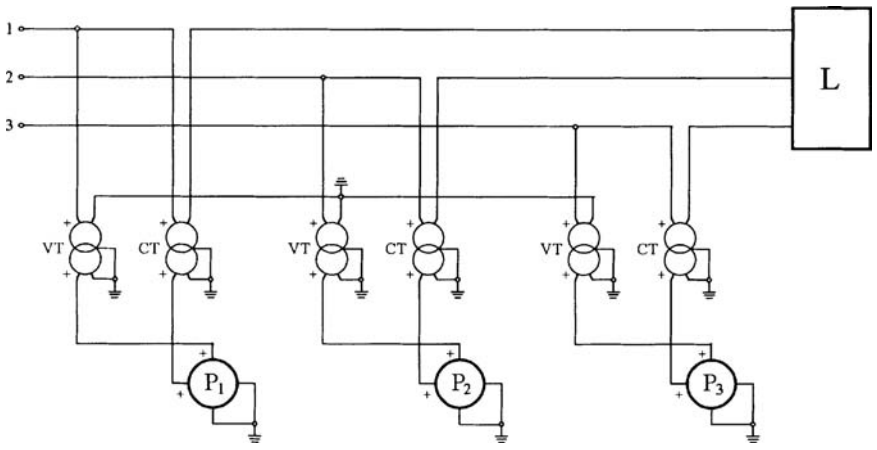

FIGURE 3.25 Medium-voltage, three-wattmeters insertion.

High-Frequency Power Measurements

Meters used for power measurements at radio or microwave frequencies are generally classified as *absorption type* (containing inside their own load, generally 50 Ω for RF work) and *transmitted* or *throughline type* (where the load is remote from the meter). Apart from the type, power meters are mainly based on thermistors, thermocouples, diodes, or radiation sensors. Therefore, to work properly, the sensor should sense all the RF power (P_{LOAD}) incoming into the sensor itself. Nevertheless, line-to-sensor impedance mismatches cause partial reflections of the incoming power ($P_{INCIDENT}$) so that a meter connected to a sensor does not account for the total amount of reflected power ($P_{REFLECTED}$). The relationship existing among power dissipated on the load, power incident, and power reflected is obviously:

$$P_{LOAD} = P_{INCIDENT} - P_{REFLECTED} \tag{3.61}$$

Directional couplers are instruments generally used for separating incident and reflected signals so that power meters can measure each of them separately. In Figure 3.27, the longitudinal section of a directional coupler for waveguides is sketched. It is made up by two waveguides properly coupled through two holes. The upper guide is the *primary waveguide* and connects the power source and load; the lower guide is the *secondary waveguide* and is connected to the power meter. To explain the working of directional couplers, incident and reflected waves have been sketched separately in Figure 3.27(a) and 3.27(b). In particular, section a depicts a directional coupler working as incident wave separator, whereas section (b) shows the separation of the reflected wave. The correct working is based on the assumption that the distance between the holes matches exactly *one quarter of the wave length* (λ). In fact, in the secondary waveguide, each hole will give rise to two waves going in opposite directions (one outside and the other inside the waveguide); consequently, in front of each hole, two waves are summed with their own phases. The assumption made on the distance between the holes guarantees that, in front of one hole, (1) the two waves propagating outside the waveguide will be in phase, causing an enforcing effect in that direction; (2) while, in front of the other hole, the two waves (always propagating outside) will be in opposition, causing a canceling effect in that direction. The enforcing and canceling effects for incident and reflected waves are opposite. In particular, according to the directions chosen in Figure 3.27, incident power propagates on the right side and is canceled on the left side (Figure 3.27(a)), while reflected power propagates on the left side and is canceled on the right side (Figure 3.27(b)). Therefore, directional couplers allow separate measurement of incident and reflected power by means of power meters applied, respectively, on the right and on the left side of the secondary waveguide.

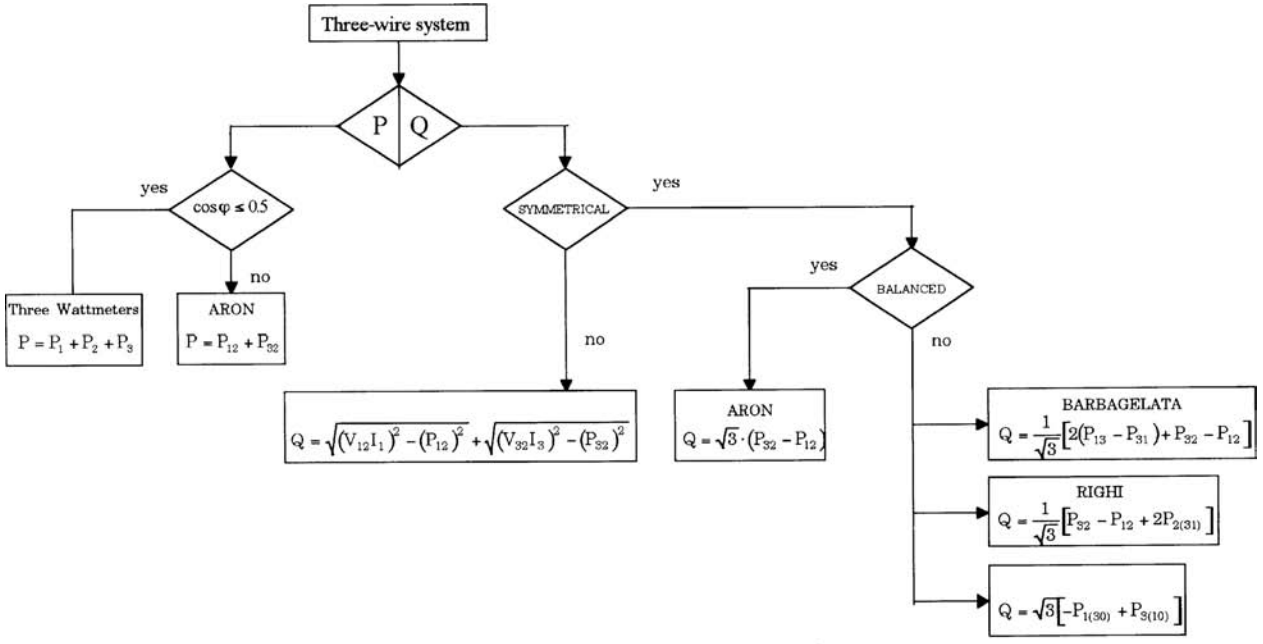

FIGURE 3.26 Method selection guide for power measurements on three-wire systems.

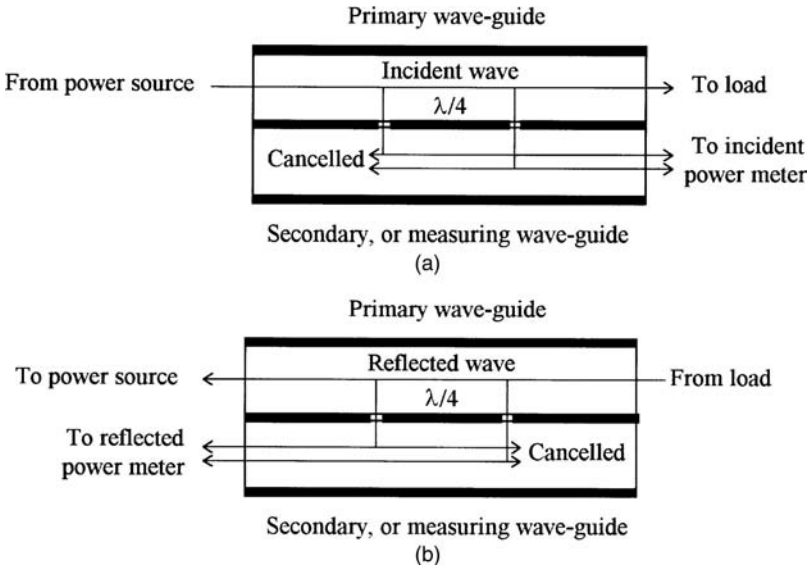

FIGURE 3.27 Directional couplers for separating incident (a) from reflected (b) power.

In any case, the secondary waveguide must be correctly matched from the impedance point of view at both sides (by adaptive loads and/or a proper choice of the power meter internal resistance) in order to avoid unwanted reflections inside the secondary waveguide.

Directional couplers are also used to determine the *reflection coefficient* ρ of the sensor, which takes into account mismatch losses and is defined as:

$$P_{\text{REFLECTED}} = \rho^2 \times P_{\text{INCIDENT}} \tag{3.62}$$

In order to take into account also the absorptive losses due to dissipation in the conducting walls of the sensor, leakage into instrumentation, power radiated into space, etc., besides the reflection coefficient, the *effective efficiency* η_C of the sensor should also be considered. Generally, the reflection coefficient and effective efficiency are included into the *calibration factor K*, defined as:

$$K = \eta_C\left(1-\rho^2\right) \times 100 \tag{3.63}$$

For example, a calibration factor of 90% means that the meter will read 10% below the incident power. Generally, calibration factors are specified by sensor manufacturers at different values of frequency.

Thermal Methods

In this section, the main methods based on power dissipation will be examined, namely: (1) thermistor-based, (2) thermocouple-based, and (3) calorimetric.

Thermistor-Based Power Meters

A thermistor is a resistor made up of a compound of highly temperature-sensitive metallic oxides [14]. If it is used as a sensor in a power meter, its resistance becomes a function of the temperature rise produced by the applied power. In Figure 3.28, typical power-resistance characteristics are reported for several values of the operating temperature.

The working principle of the thermistor power meter is illustrated in Figure 3.29 [15]: two thermistors (R_{T1} and R_{T2}) are connected (1) in parallel, for measurand signals appearing at the RF input (P_{RF}); and (2) in series, for the following measuring circuit (e.g., a bridge). The capacitance C_1 prevents the power dc component from flowing to the thermistors; the C_2 stops the RF power toward the bridge.

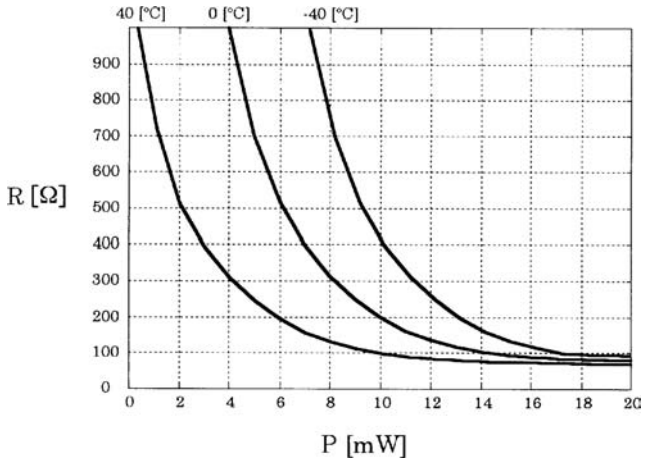

FIGURE 3.28 Typical power-resistance characteristics of commercial thermistors.

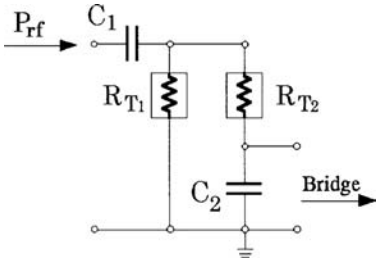

FIGURE 3.29 Working principle of the thermistor-based power meter.

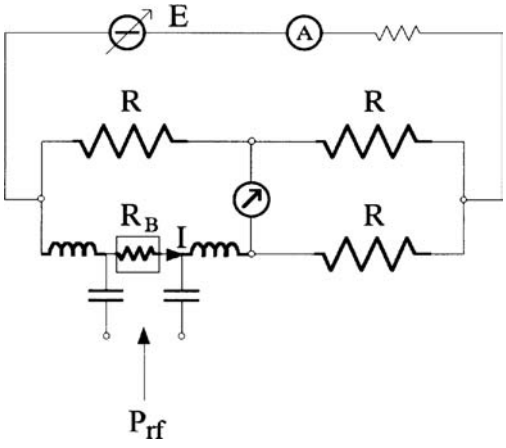

FIGURE 3.30 The manual bolometer.

A bridge with a thermistor or a barretter in one arm is called a *bolometer*. Bolometer-based measurements can be performed with (1) a manual bolometer with variation of the bias current, (2) a manual bolometer with substitution method, or (3) a self-balancing bolometer.

The *manual bolometer with a variation of the bias current* is illustrated in Figure 3.30. Its working principle consists of two steps. In the first, no RF power is applied to the sensor; the equilibrium is obtained by varying the dc power supply E until the sensor resistance R_B, related to the dc power flowing

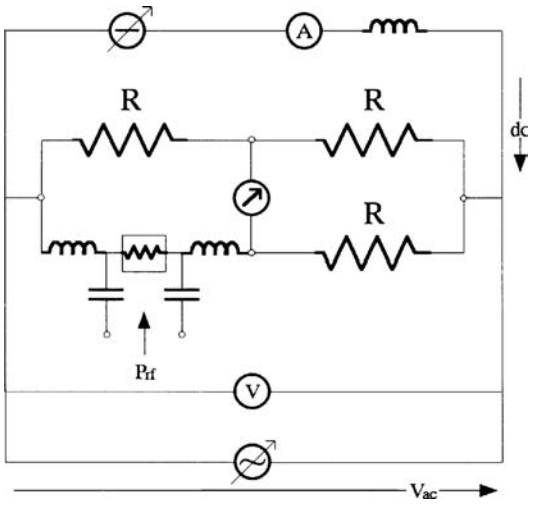

FIGURE 3.31 Manual bolometer with substitution method.

in it, is equal to R. In this condition, let the current I flowing into the sensor be equal to I_1. In the second step, an RF power P_{RF} is fed to the sensor; the power increase must be compensated by a dc power decrease, which is performed by lowering the bridge dc supply voltage E; in this case, let I be equal to I_2.

Since the power dissipated in the sensor has been maintained constant in both steps, the power P_{RF} can be evaluated as:

$$P_{RF} = \frac{R}{4}\left(I_1^2 - I_2^2\right) \tag{3.64}$$

The *manual bolometer with substitution method* (Figure 3.31) consists of two sequential steps; in the first, both RF power (P_{RF}) and dc power (P_{dc}) are present, and the power (P_d) necessary to lead the bridge to the equilibrium is:

$$P_d = P_{dc} + P_{RF} \tag{3.65}$$

During the second step, P_{RF} is set to zero and an alternative voltage V_{ac} is introduced in parallel to the dc power supply. In this case, the power P_d necessary to balance the bridge:

$$P_d = P_{dc} + P_{ac} \tag{3.66}$$

is obtained by varying v_{ac}.

Since P_d is the same in both cases, the power supplied by the alternative generator is equal to P_{RF}:

$$P_{RF} = P_{ac} = \frac{V_{ac}^2}{4R} \tag{3.67}$$

Equation 3.66 implies that the RF power can be obtained by a voltage measurement. The *self-balancing bolometer* (Figure 3.32) automatically supplies a dc voltage V to balance the voltage variations due to sensor resistance R_B changes for an incident power P_{RF}. At equilibrium, R_B is equal to R and the RF power will then be:

$$P_{RF} = \frac{V^2}{4R} \tag{3.68}$$

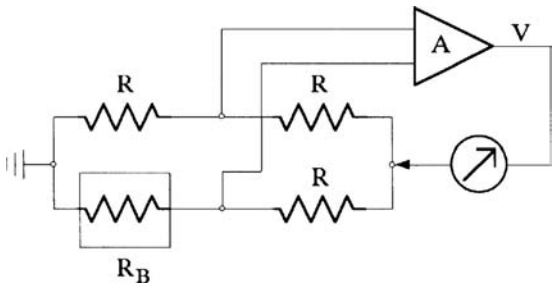

FIGURE 3.32 Self-balancing bolometer.

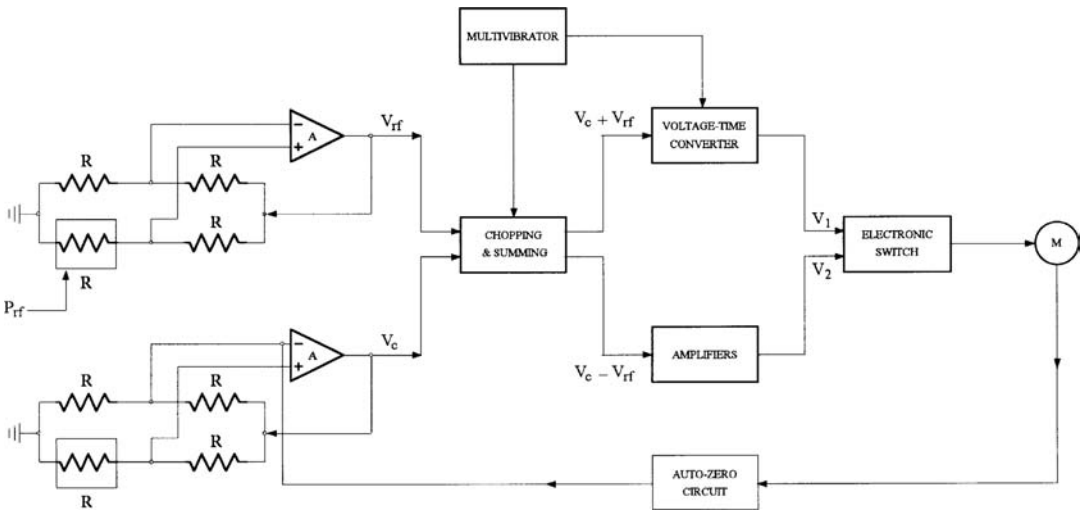

FIGURE 3.33 Power meter based on two self-balancing bridges.

As mentioned above, the thermistor resistance depends on the surrounding temperature. This effect is compensated in an instrument based on two self-balancing bridges [15]. The RF power is input only to one of these, as shown in Figure 3.33.

The equilibrium voltages V_c and V_{RF} feed a chopping and summing circuit, whose output $V_c + V_{RF}$ goes to a voltage-to-time converter. This produces a pulse train V_1, whose width is proportional to $V_c + V_{RF}$. The chopping section also generates a signal with an amplitude proportional to $V_c - V_{RF}$, and a frequency of a few kilohertz, which is further amplified. The signals V_1 and V_2 enter an electronic switch whose output is measured by a medium value meter M. This measure is proportional to the RF power because:

$$P_{RF} = \frac{(V_c + V_{RF})(V_c - V_{RF})}{4R} \Rightarrow P_{RF} = \frac{V_c^2 - V_{RF}^2}{4R} \tag{3.69}$$

Owing to the differential structure of the two bolometers, this device is capable of performing RF power measurements independent of the surrounding temperature. In addition, an offset calibration can be carried out when P_{RF} is null and V_c is equal to V_{RF}.

These instruments can range from 10 mW to 1 μW and utilize sensors with frequency bandwidths ranging from 10 kHz to 100 GHz.

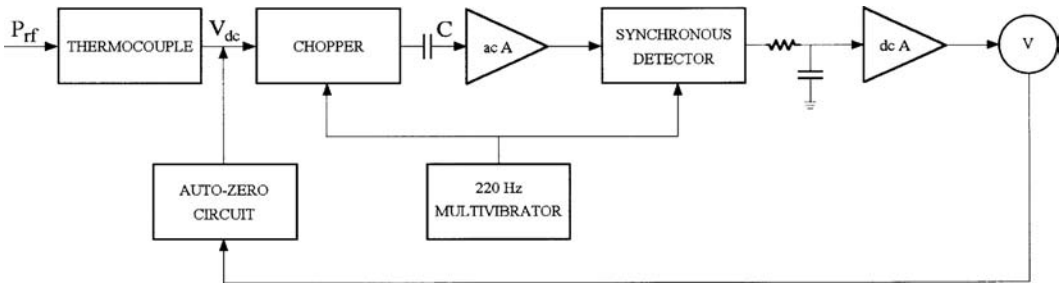

FIGURE 3.34 Power meter with thermocouple-based sensor.

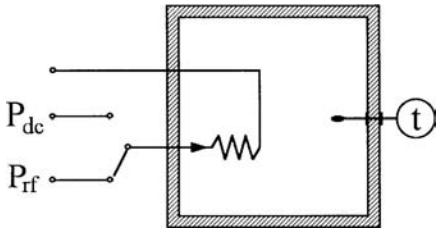

FIGURE 3.35 Calorimetric method based on a substitution technique.

Thermocouple-Based Power Meters

Thermocouples [14] can be also used as RF power meters up to frequencies greater than 40 GHz. In this case, the resistor is generally a thin-film type. The sensitivity of a thermocouple can be expressed as the ratio between the dc output amplitude and the input RF power. Typical values are 160 μV mW^{-1} for minimum power of about 1 μW.

The measure of voltages of about some tens of millivolts requires strong amplification, in that the amplifier does not have to introduce any offset. With this aim, a chopper microvoltmeter is utilized [16], as shown in the Figure 3.34.

The thermocouple output voltage V_{dc} is chopped at a frequency of about 100 Hz; the resulting square wave is filtered of its mean value by the capacitor C and then input to an ac amplifier to further reduce offset problems. A detector, synchronized to the chopper, and a low-pass filter transform the amplified square voltage in a dc voltage finally measured by a voltmeter.

Calorimetric Method

For high frequencies, a substitution technique based on a calorimetric method is utilized (Figure 3.35) [17]. First, the unknown radio frequency power P_{RF} is sent to the measuring device t, which measures the equilibrium temperature. Then, once the calorimetric fluid has been cooled to its initial temperature, a dc power P_{dc} is applied to the device and regulated until the same temperature increase occurs in the same time interval. In this way, a thermal energy equivalence is established between the known P_{dc} and the measurand P_{RF}.

A comparison version of the calorimetric method is also used for lower frequency power measurements (Figure 3.36). The temperature difference ΔT of a cooling fluid between the input (1) and the output (2) sections of a cooling element where the dissipated power to be measured P is determined. In this case, the power loss will correspond to P:

$$P = C_p \rho Q \Delta T \tag{3.70}$$

where C_p is the specific heat, ρ the density, and Q the volume flow, respectively, of the refreshing fluid.

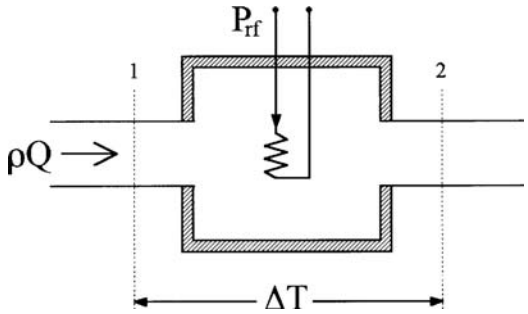

FIGURE 3.36 Calorimetric method based on a comparison technique.

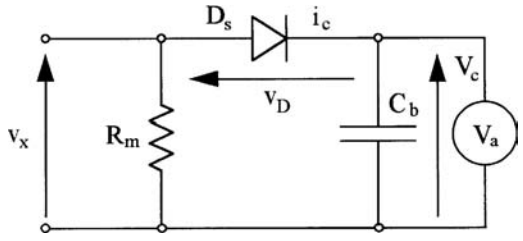

FIGURE 3.37 Circuit of the diode sensor-based power measurement.

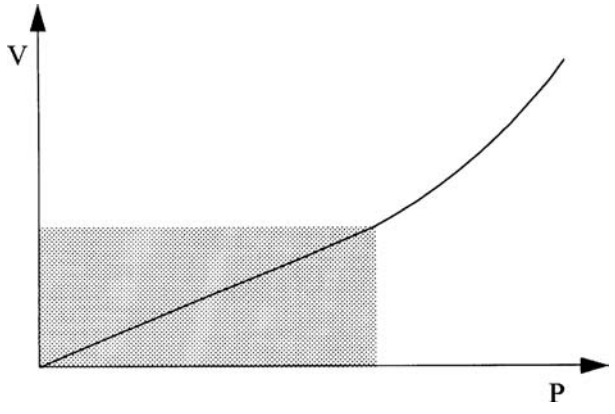

FIGURE 3.38 Characteristic of a low-barrier Schottky diode.

Diode Sensor-Based Power Measurements

Very sensitive (up to 0.10 nW, –70 dBm), high-frequency (10 MHz to 20 GHz) power measurements are carried out through a diode sensor by means of the circuit in Figure 3.37 [18]. In particular, according to a suitable selection of the components in this circuit, (1) true-average power measurements, or (2) peak power measurements can be performed.

The basic concept underlying *true-average power measurements* exploits the nonlinear squared region of the characteristic of a low-barrier Schottky diode (nondashed area in Figure 3.38). In this region, the current flowing through the diode is proportional to the square of the applied voltage; thus, the diode acts as a squared-characteristic sensor.

In the circuit of diode sensor-based wattmeters shown in Figure 3.37, the measurand v_x, terminated on the matching resistor R_m, is applied to the diode sensor D_s working in its squared region in order to produce a corresponding output current i_c in the bypass capacitor C_b. If C_b has been suitably selected,

the voltage V_c between its terminals, measured by the voltmeter amplifier V_a, is proportional to the average of i_c, i.e., to the average of the squares of instantaneous values of the input signal v_x, and, hence, to the true average power.

In the true-average power measurement of nonsinusoidal waveforms having the biggest components at low frequency, such as radio-frequency AM (Amplitude Modulated), the value of C_b must also satisfy another condition. The voltage v_d on the diode must be capable of holding the diode switched-on into conduction even for the smallest values of the signal. Otherwise, in the valleys of the modulation cycle, the high-frequency modulating source is disconnected by the back-biased diode and the measurement is therefore misleading.

On the other hand, for the same signal but for a different selection of the C_b value, the circuit can act as a peak detector for *peak power measurements*. As a matter of fact, the voltage v_c on the bypass capacitor C_b during the peak of the modulation cycle is so large that in the valleys, the high-frequency peaks are not capable of switching on the diode into conduction; thus, these peaks do not contribute to the measured power level.

If higher power levels have to be measured (10 mW to 100 mW), the sensing diode is led to work out of the squared region into its linear region (dashed area in Figure 3.38). In this case, the advantage of true-average power measurements for distorted waveforms is lost; and for peak power measurements, since the diode input-output characteristic is nonlinear and the output is squared, spectral components different from the fundamental introduce significant measuring errors.

Radiation Sensor-Based Power Measurements

Very high-frequency power measurements are usually carried out by measuring a radiant flux of an electromagnetic radiation through a suitable sensor. In particular, semiconductor-based radiation microsensors have gained wider and wider diffusion [19], in that size reduction involves several well-known advantages such as greater portability, fewer materials, a wider range of applications, etc. One of the most familiar applications of radiation sensor-based power measurements is the detection of object displacement. Furthermore, they are also commonly used for low-frequency power noninvasive measurements.

Radiation sensors can be classified according to the measurand class to which they are sensitive: nuclear particles or electromagnetic radiations. In any case, particular sensors capable of detecting both nuclear particles and electromagnetic radiations, such as gamma and X-rays, exist and are referred to as nucleonic detectors.

In Table 3.1, the different types of radiation sensors utilized according to the decrease of the measurand wavelength from microwaves up to nuclear (X, gamma, and cosmic) rays are indicated.

In particular, *microwave* power radiation sensors are mainly used as noncontacting detectors relying on ranging techniques using microwaves [20]. Shorter and longer (radar) wavelength microwave devices are employed to detect metric and over-kilometer displacements, respectively.

Beyond applications analogous to microwave, power radiation *infrared* sensors also find use as contact detectors. In particular, there are two types of infrared detectors: thermal and quantum. The thermal type includes contacting temperature sensors such as thermocouples and thermopiles, as well as noncontacting pyroelectric detectors. On the other hand, the quantum type, although characterized by a strong wavelength dependence, has a faster response and includes photoconductive (spectral range: 1 μm to 12 μm) and photovoltaic (0.5 μm to 5.5 μm) devices.

The main power radiation *visible and ultraviolet* sensors are photoconductive cells, photodiodes, and phototransistors. Photodiodes are widely used to detect the presence, the intensity, and the wavelength of light or ultraviolet radiations. Compared to photoconductive cells, they are more sensitive, smaller, more stable and linear, and have lower response times. On the other hand, phototransistors are more sensitive to light.

At very low light levels, rather than silicon-based microsensors, *nuclear radiation* power microsensors are needed. In this case, the most widespread devices are scintillation counters, solid-state detectors, plastic films, and thermoluminescent devices. The scintillation counter consists of an active material that

TABLE 3.1 Operating Field of Main Radiation Power Sensors

Operating Field (Wavelength)	Microwave (1, 10^{-3} m)	Infrared (10^{-3}, 10^{-6} m)	Visible and Ultraviolet (10^{-6}, 10^{-9} m)	Nuclear Rays (10^{-8}, 10^{-15} m)
Sensors	Noncontacting displacement sensors	Pyroelectric, photoconductive, photovoltaic	Photoconductive, photovoltaic	Scintillation counters, plastic films, solid-state, thermolum

converts the incident radiation to pulses of light, and a light-electric pulse converter. The active material can be a crystal, a plastic fluorine, or a liquid. The scintillator size varies greatly according to the radiation energy, from thin solid films to large tanks of liquid to detect cosmic rays. A thin (5 μm) plastic polycarbonate film or a thermoluminescent material (e.g., LiF) can measure the radiation power falling on a surface. The film is mechanically damaged by the propagation of highly α–ionizing particles. Consequent etching of the film reveals tracks that can be observed and counted.

3.3 Pulse Power Measurements

Pulse waveforms are becoming more and more diffused in several fields such as telecommunications, power source applications, etc. The *pulse power* P_p is defined as the average power P_m in the pulse width:

$$P_p = \frac{P_m}{\tau_d} \tag{3.71}$$

where τ_d is the duty cycle of the pulse waveform (i.e., the pulse width divided by the waveform period). If the pulse width cannot be accurately defined (e.g., nonrectangular pulses in the presence of noise), the pulse power P_p becomes unmeaningful. In this case, the *peak envelope power* is introduced as the maximum of the instantaneous power detected on a time interval, including several periods of the pulse waveform (but negligible with respect to the modulation period, in the case of PWM waveforms).

Several techniques are used to measure pulse power [21]. In particular, they can be classified according to the *pulse frequency* and the necessity for *constraining real-time applications* (i.e., measuring times, including a few of the modulation periods). For real-time, low-frequency applications (up to 100 kHz), the algorithms mentioned in the above sections on wattmeters based on digital multipliers can be applied [9].

If constraining limits of real-time do not have to be satisfied, either digital or analog techniques can be utilized. As far as the digital techniques are concerned, for high-frequency applications, if the measurand pulse waveform is stationary over several modulation periods, digital wattmeters based on equivalent sampling can be applied, with accuracies increasing according to measuring times. As far as the analog techniques are concerned, three traditional methods are still valid: (1) average power per duty cycle, (2) integration-differentiation, and (3) dc/pulse power comparison.

A block diagram of an instrument measuring *average power per duty cycle* is illustrated in Figure 3.39. At first, the mean power of the measurand pulse signal, terminated on a suitable load, is measured by means of an average power meter; then, the pulse width and the pulse waveform period are measured by a digital counter. Finally, the power is obtained by means of Equation 3.71.

The *integration-differentiation* technique is based on a barretter sensor capable of integrating the measurand, and on a conditioning and differentiating circuit to obtain a voltage signal proportional to the measurand power. The signal is input to the barretter sensor, having a thermal constant such that the barretter resistance will correspond to the integral of the input. The barretter is mounted as an arm of a conditioning Wheatstone bridge; in this way, the barretter resistance variations are transformed into voltage variations, and an integrated voltage signal is obtained as an output of the bridge detecting arm. This signal, suitably integrated to reach a voltage signal proportional to the output, is detected by a peak

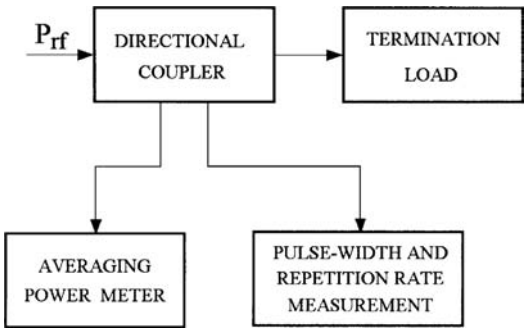

FIGURE 3.39 Block diagram of an instrument measuring average power per duty cycle.

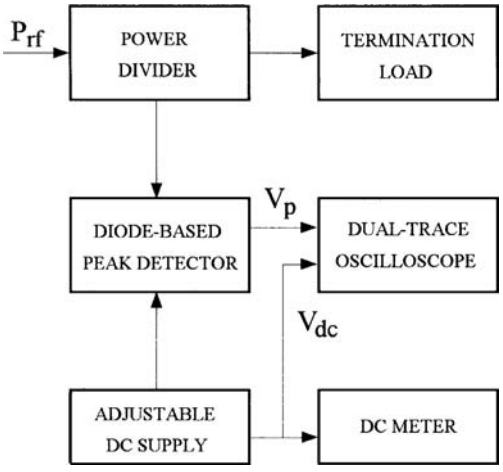

FIGURE 3.40 Block diagram of an instrument based on dc/pulse power comparison technique.

voltmeter calibrated in power. Analogously to the selection of the time constant of an *RC* integrating circuit, attention must be paid to the thermal constant selection of the barretter in order to attain the desired accuracy in the integration. With respect to the measurand pulse period, a very long thermal constant will give rise to insufficient sensitivity. On the other hand, a very short constant approaching the pulse duration will give rise to insufficient accuracy.

The *dc/pulse power comparison* technique is based on the concept of first revealing the peak envelope power through a diode sensor, and then comparing the peak to a known dc source with a dual trace scope. A block diagram of an instrument based on this concept is illustrated in Figure 3.40. The peak of the measurand pulse signal terminated on a suitable load is sensed by a peak detector by obtaining a proportional signal V_p. This signal is input to a channel of a dual trace oscilloscope and the envelope peak is displayed. An adjustable dc source is input to the other channel of the scope to obtain a signal V_{dc} to be compared to the envelope peak signal. When the two signals are made equal, a dc voltage meter directly calibrated in peak power measures the output power.

References

1. G. Zingales, Power measurements on single-phase ac circuits (Chap. VI, 6.2), in *Methods and Instruments for Electrical Measurements*, (in Italian), Torino: UTET, 1980.
2. G. Korànyi, Measurement of power and energy, in L. Schnell (Ed.), *Technology of Electrical Measurements*, Chichester: John Wiley & Sons, 1993.

3. J. Milmann and C.C. Halkias, *Integrated Electronics: Analog and Digital Circuits and Systems,* New York: McGraw-Hill, 1972.
4. F.F. Mazda, Ac analogue instruments (Chap. VI, 6.3), in *Electronic Instruments and Measurement Techniques*, Cambridge, U.K.: Cambridge University Press, 1987.
5. P.S. Filipski, A TDM wattmeter with 0.5 MHz carrier frequency, *IEEE Trans. Instrum. Meas.*, IM39, 15-18, 1990.
6. J.R. Carstens, *Electrical Sensors and Transducers*, Englewood Cliffs, NJ: Prentice-Hall, 1992.
7. Lu Zu-Liang, An error estimate for quasi-integer-period sampling and an approach for improving its accuracy, *IEEE Trans. Instrum. Meas.*, IM-23, 337-341, 1984.
8. V. Haasz, The error analysis of digital measurements of electrical power, *Measurement*, 6, 1986.
9. P. Arpaia, F. Avallone, A. Baccigalupi, and C. De Capua, Real-time algorithms for active power measurements on PWM-based electric drives, *IEEE Trans. Instrum. Meas.*, IM-45, 462-466, 1996.
10. X. Dai and R. Gretsch, Quasi-synchronous sampling algorithm and its applications, *IEEE Trans. Instrum. Meas.*, IM-43, 204-209, 1994.
11. M. Bellanger, *Digital Processing of Signals: Theory and Practice*, Chichester: John Wiley & Sons, 1984.
12. M. Bertocco, C. Offelli, and D. Petri, Numerical algorithms for power measurements, *Europ. Trans. Electr. Power*, ETEP 3, 91-101, 1993.
13. G. Zingales, Measurements on steady-state circuits (Chap. VI), in *Methods and Instruments for Electrical Measurements* (In Italian), Torino: UTET, 1980.
14. H.N. Norton, Thermometers (Chap. 19), in *Handbook of Transducers*, Englewood Cliffs, NJ: Prentice-Hall, 1989.
15. Anonymous, Thermistor mounts and instrumentation (Chap. II), in *Fundamental of RF and Microwave Power Measurements,* Application Note 64-1, Hewlett Packard, 1978.
16. R.E. Pratt, Power measurements (15.1–15.16), in C.F. Coombs (Ed.), in *Handbook of Electronic Instruments*, New York: McGraw-Hill, 1995.
17. F. F. Mazda, High-frequency power measurements (Chap. VIII, 8.4), in *Electronic Instruments and Measurement Techniques*, Cambridge: Cambridge University Press, 1987.
18. Anonymous, Diode detector power sensors and instrumentation (Chap. IV), in *Fundamental of RF and Microwave Power Measurements,* Application Note 64-1, Hewlett Packard, 1978.
19. J.W. Gardner, *Microsensors: Principles and Applications,* Chichester: John Wiley & Sons, 1994.
20. H.N. Norton, Radiation pyrometers (Chap. 20), in *Handbook of Transducers*, Englewood Cliffs, NJ: Prentice-Hall, 1989.
21. F.F. Mazda, Pulse power measurement (Chap. VIII, 8.5), in *Electronic Instruments and Measurement Techniques,* Cambridge, U.K.: Cambridge University Press, 1987.

Further Information

F.K. Harris, The Measurement of Power (Chap. XI), in *Electrical Measurements*, Huntington, NY: R.E. Krieger Publishing, 1975; a clear reference for line-frequency power measurements.

Anonymous, *Fundamental of RF and Microwave Power Measurements,* Application Note 64-1, Hewlett Packard, 1978; though not very recent, is a valid and comprehensive reference for main principles of high-frequency power measurements.

J.J. Clarke and J.R. Stockton, Principles and theory of wattmeters operating on the basis of regularly spaced sample pairs, *J. Phys. E. Sci. Instrum.*, 15, 645-652, 1982; gives basics of synchronous sampling for digital wattmeters.

T.S. Rathore, Theorems on power, mean and RMS values of uniformly sampled periodic signals, *IEE Proc. Pt. A*, 131, 598-600, 1984; provides fundamental theorems for effective synchronous sampling wattmeters.

J.K. Kolanko, Accurate measurement of power, energy, and true RMS voltage using synchronous counting, *IEEE Trans. Instrum. Meas.*, IM-42, 752–754, 1993; provides information on the implementation of a synchronous dual-slope wattmeter.

G.N. Stenbakken, A wideband sampling wattmeter, *IEEE Trans. Power App. Syst.*, PAS-103, 2919-2925, 1984; gives basics of asynchronous sampling-based wattmeters and criteria for computing uncertainty in time domain.

F. Avallone, C. De Capua, and C. Landi, Measurement station performance optimization for testing on high efficiency variable speed drives, *Proc. IEEE IMTC/96* (*Brussels, Belgium*), 1098–1103, 1996; proposes an analytical model of uncertainty arising from power measurement systems working under highly distorted conditions.

F. Avallone, C. De Capua, and C. Landi, Metrological performance improvement for power measurements on variable speed drives, *Measurement*, 21, 1997, 17-24; shows how compute uncertainty of measuring chain components for power measurements under highly distorted conditions.

F. Avallone, C. De Capua, and C. Landi, Measurand reconstruction techniques applied to power measurements on high efficiency variable speed drives, *Proc. of XIV IMEKO World Congress* (*Tampere, Fi*), 1997; proposes a technique to improve accuracy of power measurements under highly distorted conditions.

F. Avallone, C. De Capua, and C. Landi, A digital technique based on real-time error compensation for high accuracy power measurement on variable speed drives, *Proc. of IEEE IMTC/97* (*Ottawa, Canada*), 1997; reports about a real-time technique for error compensation of transducers working under highly distorted conditions.

J.C. Montano, A. Lopez, M. Castilla, and J. Gutierrrez, DSP-based algorithm for electric power measurement, *IEE Proc. Pt.A*, 140, 485–490, 1993; describes a Goertzel FFT-based algorithm to compute power under nonsinusoidal conditions.

S.L. Garverick, K. Fujino, D.T. McGrath, and R.D. Baertsch, A programmable mixed-signal ASIC for power metering, *IEEE J. Solid State Circuits*, 26, 2008–2015, 1991; reports about a programmable mixed analog-digital integrated circuit based on six first-order sigma-delta ADCs, a bit serial DSP, and a byte-wide static RAM for power metering.

G. Bucci, P. D'Innocenzo, and C. Landi, A modular high-speed dsp-based data acquisition apparatus for on-line quality analysis on power systems under non-sinusoidal conditions, *Proc. of 9th IMEKO TC4 Int. Sym.* (Budapest, Hungary), 286–289, 1996; shows the strategy of measurement system design for power measurements under non-sinusoidal conditions.

K.K. Clarke and D.T. Hess, A 1000 A/20 kV/25 kHz-500 kHz volt-ampere-wattmeter for loads with power factors from 0.001 to 1.00, *IEEE Trans. Instrum. Meas.*, IM-45, 142-145, 1996; provides information on the implementation of an instrument to perform an accurate measurement of currents (1 A to 1000 A), voltages (100 V to 20 kV), and powers (100 W to 20 MW) over the frequency range from 25 kHz to 500 kHz.

P. Arpaia, G. Betta, A. Langella, and M. Vanacore, An Expert System for the Optimum Design of Measurement Systems, *IEE Proc.* (*Pt. A*), 142, 330–336, 1995; reports about an Artificial Intelligence tool for the automatic design of power measuring systems.

In any case, *IEEE Transactions on Instrumentation and Measurement* and *Measurement* journals provide current research on power measurements.